

Analysis of Surface Integrity in Dry and Cryogenic Machining of AZ31B Mg Alloys

Z. Pu^{1, a}, S. Caruso^{2, b}, D. Umbrello^{2, c}, O. W. Dillon, Jr.^{1, d}, D.A. Puleo^{3, e},
I.S. Jawahir^{1, f}

¹University of Kentucky, Institute for Sustainable Manufacturing and Department of Mechanical Engineering, 523 CRMS Building, Lexington, KY 40506, USA

²University of Calabria, Department of Mechanical Engineering, 87036 Rende (CS), Italy

³University of Kentucky, Center for Biomedical Engineering, Wenner-Gren Lab, Lexington, Kentucky, USA

^azpu2@engr.uky.edu, ^bserafino.caruso@unical.it, ^cd.umbrello@unical.it, ^dvzn05xpm@verizon.net,
^epuleo@uky.edu, ^fjawahir@engr.uky.edu

Keywords: Cryogenic machining, surface integrity, severe plastic deformation, grain refinement, DRX, FEM, magnesium alloys

Abstract. Surface integrity of machined products can have a critical impact on their performance, such as corrosion, wear and/or fatigue resistance. It has been reported that reducing the grain size of *AZ31B Mg* alloys could significantly enhance its corrosion resistance, which is often the limiting factor for its wide application. Severe plastic deformation (SPD) has proved to be an effective way to induce grain refinement. In this study, the potential of cryogenic machining as a novel SPD method to induce grain refinement on the surface of *AZ31B Mg* alloys was investigated. The microstructures of the workpiece surface/sub-surface and the machined chips after both dry and cryogenic machining were studied. A surface layer where nanocrystallized grains exist was found in the machined surface under cryogenic conditions. Increasing the edge radius of the cutting tool resulted in a thicker grain refinement layer. In addition to the experimental study, an FE model based on the Johnson-Cook constitutive equation was developed and validated using experimental data in terms of chip morphology and forces. The capability of this model to predict critical deformation parameters for dynamic recrystallization (DRX), such as strain, strain-rate and temperature, was demonstrated. With further development, the model can be used to predict the onset of DRX and the grain size on the machined surface.

Introduction

Surface integrity of the machined product can have a critical impact on its performance, especially the properties that are sensitive to the surface conditions, such as corrosion, wear and/or fatigue resistance. Grain refinement down to the nano/ultrafine level in the surface and sub-surface induced by severe plastic deformation (SPD) has proved to be an effective method of enhancing the performance of components. Surface nanocrystallization (SNC) of *1Cr18Ni9Ti* stainless steel induced by high-energy shot peening was reported to enhance its corrosion resistance remarkably [1]. A 50% enhancement in the fatigue endurance of a nickel-based Hastelloy C-2000 was achieved after the grain size on the surface was reduced to 22 nm by a SNC process [2].

Magnesium alloys have been considered as a promising lightweight structural material for both automotive and aerospace applications for a long time. Recently, new application of magnesium alloys as a novel biodegradable material for temporary internal fixation implants is also emerging [3]. However, one major limitation of the wide application has been their unsatisfactory corrosion performance.

The potential of grain refinement by SPD on improved corrosion resistance has not been fully investigated. Alvarez-Lopez et al. [4] reported that *AZ31 Mg* alloy samples with 4.5 μm grain size processed by equal channel angular presses (ECAP) followed by rolling had better corrosion resistance than the initial samples which had 25.7 μm grains in simulated body fluid (SBF).

Most of the current SNC processes involve repetitive impacts of balls, which may increase the surface roughness significantly and introduce cracks. The surface roughness after a SNC process was increased from 0.41 μm to 5.5 μm [2]. Both increase and decrease of corrosion resistance of AISI 409 stainless steel were reported after a surface mechanical attrition treatment (SMAT) [5].

Machining is a SPD process involving large shear strain (typically 2–10) and high strain rates (up to 10^6 s^{-1}). Dynamic recrystallization (DRX) occurs under proper machining conditions and ultrafine/nano grain structures were produced in both machined chips [6] and the machined surface [7]. However, due to the large amount of heat generated during machining, recrystallized grain tends to grow and the thickness of the grain refinement layer is very small. Only very mild cutting conditions can be used to reduce heat generation [7]. Liquid nitrogen was used during friction stir processing (FSP) of *AZ31 Mg* alloy, resulting in significant grain refinement from around 75 μm to 100–300 nm [8].

In this study, the potential of cryogenic machining whereby liquid nitrogen is sprayed directly onto the machined surface to suppress grain growth after DRX in the surface and sub-surface layers is studied. The microstructures after both dry and cryogenic machining are investigated. The influence of cooling method and edge radius of cutting tools is discussed.

In addition to the experimental studies, an FE model using the Johnson-Cook constitutive equation is developed to simulate orthogonal turning of *AZ31B Mg* alloy under dry conditions. Experimental data, including the chip morphology, cutting and radial forces, are used to validate the model.

Since both the onset of DRX and the grain size after DRX are dependent on deformation parameters, such as strain, strain-rate and temperature [9], studying the influence of machining conditions on these parameters is a critical step towards controlling the microstructure after machining. In the current study, the validated FE model is used to investigate the influence of edge radius of cutting tools on strains in the surface and sub-surface of the workpiece.

Experimental and Numerical Procedures

Experimental Procedures. The work material studied was the commercial *AZ31B-O* magnesium alloy. It was obtained in the form of a 3 mm thick sheet. Disc specimens were made from the sheet (3 mm in thickness and 130 mm in diameter) and subsequently subjected to orthogonal machining. It is noted that turning is used as the final step to prepare the discs from the sheet in the machine shop.

A Mazak Quick Turn-10 Turning Center equipped with an Air Products ICEFLY® liquid nitrogen delivery system is used to conduct orthogonal turning on the *AZ31 Mg* discs. As shown in Fig. 1, liquid nitrogen was sprayed to the machined surface from the clearance side of the cutting tool during cryogenic machining. A KISTLER 3-Component Tool Dynamometer was used to monitor the cutting and radial forces during machining.

The cutting tool used was uncoated carbide C5/C6 inserts from Kennametal. The edge radius of the cutting tools (r_n) was ground to two different values. The actual tool edge radius before machining was measured using a ZYGO New View 5300 measurement system.

The experimental matrix is shown in Table 1. Edge radius is a key factor addressed in this study since it was reported to have significant influence on the surface integrity of machined products, especially residual stresses [10]. The rake angle is kept constant at -7° .

After machining, metallurgical samples were cut from the machined discs. After cold mounting, grinding and polishing, acetic picric solution was used as the etchant to reveal the grain structure. Optical microscopy was used to observe the microstructure of the *AZ31B Mg* discs and the machined chips.

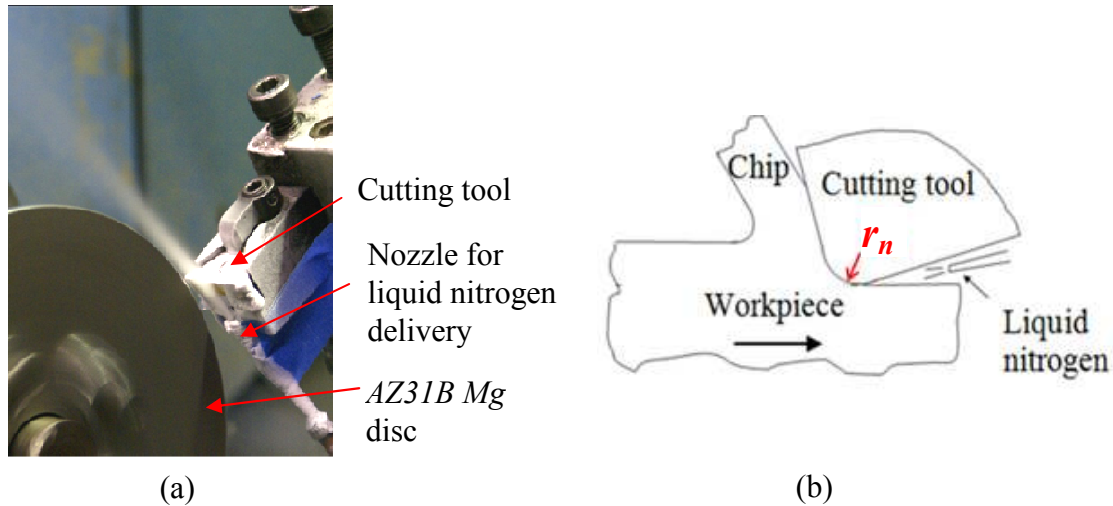


Fig. 1: (a) Photo and (b) schematic diagram of machining setup with an Air Products ICEFLY® liquid nitrogen delivery system.

Table 1: Matrix for the machining experiments

No.	Cooling Method	Tool Edge Radius [μm]	Cutting Speed [m/min]	Feed Rate [mm/rev]
1	Dry	30	100	0.1
2	Dry	67	100	0.1
3	Cryogenic	30	100	0.1
4	Cryogenic	68	100	0.1

FE numerical procedures. The commercial FEM software DEFORM-2D™, a Lagrangian implicit code, was used to simulate the orthogonal cutting process of AZ31B Mg alloy. The workpiece was initially meshed with 7000 isoparametric quadrilateral elements. The element density around the cutting edge, along the machined surface and in the machined chip was set to be much larger than the other location as shown in Fig. 2. The smallest element size is about 10 μm . The tool was meshed with 2500 elements. A plane-strain coupled thermo-mechanical analysis was performed.

The Johnson–Cook constitutive equation was implemented in the FE code by a user subroutine used to model the material behavior of AZ31B Mg alloy during machining. The equation is:

$$\sigma = (A + B \cdot \varepsilon^n) \cdot [1 + C \cdot \ln(\frac{\dot{\varepsilon}}{\dot{\varepsilon}_0})] \cdot [1 - (\frac{T - T_{room}}{T_m - T_{room}})^m] \quad (1)$$

where ε is the plastic strain; $\dot{\varepsilon}$ is the plastic strain rate (s^{-1}); $\dot{\varepsilon}_0$ is the reference plastic strain rate (s^{-1}); T is the temperature of the work material; T_m is the melting temperature of the work material and T_{room} is the room temperature (20 °C). Coefficient A is the yield strength (MPa); B is the hardening modulus (MPa); C is the strain-rate sensitivity coefficient; n is the hardening coefficient and m the thermal softening coefficient.

Hasenpouth [11] performed a wide range of mechanical testing of AZ31B Mg sheet where the strain rates varied from 0.003 s^{-1} to 1500 s^{-1} and the temperature from room temperature to 250 °C. After data fitting, the constants for Johnson-Cook constitutive model were found for both rolling and transverse directions. The constants for the FE model in this study were an average of the two directional values as shown in Table 2.

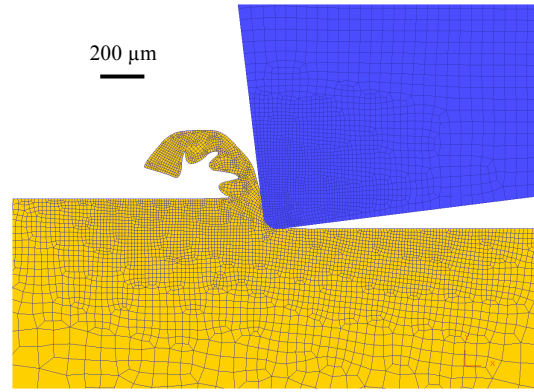


Fig. 2: Mesh for the workpiece and the tool.

Table 2: Johnson-Cook constants of *AZ31B Mg* alloy for the FE model [11]

	Rolling Direction	Transverse Direction	Average
A [Mpa]	133.082	193.762	163.422
B [Mpa]	345.821	296.834	321.328
n	0.293	0.38	0.337
C	0.016	0.016	0.016
m	1.849	1.808	1.829

The physical and thermal properties of *AZ31B Mg* alloy used in the FE model are listed in Table 3 [12].

Table 3: Physical and thermal material properties of *AZ31B Mg* alloy [12]

Density [kg/mm ³]	1.77×10 ⁻⁶
Young's Modulus [kN/mm ²]	45,000
Possion's ratio	0.35
Melting temperature [K]	891
Thermal Conductivity [W/(mK)]	77+0.096 T
Specific heat capacity [J/(kgK)]	1000+0.666T
Thermal expansion coefficient [K ⁻¹]	2.48×10 ⁻⁵

The influence of different tool-chip friction models on FEM results was investigated by Filice et al. [13] and it was found that as long as the friction coefficient was well calibrated, both cutting forces and chip morphology could be well predicted independent of which friction model was used. In this study, a simple constant shear friction model is applied:

$$\tau = m \cdot \tau_0 \quad (2)$$

where τ is the frictional stress between the tool and the chip and work material, τ_0 is the shear flow stress of the working material and m is a friction constant.

The chip morphology of Ti6Al4V alloy was successfully predicted by Umbrello [14] using the Cockroft and Latham's fracture criterion [15], which is expressed as:

$$\int_0^{\bar{\epsilon}_f} \sigma_1 d\bar{\epsilon} = D \quad (3)$$

where $\bar{\varepsilon}_f$ is the effective strain; σ_1 is the maximum principal stress; D is a material constant. When the integral of the maximum tensile principal stress component over the plastic strain path reaches the critical damage value D , fracture occurs and chip segmentation starts.

The values of m and D were determined by an iterative calibration process using the experimental data on chip morphology and forces. The studied range for m is from 0.1 to 0.7. The initial estimated value of D was found by integrating a published flow stress curve from beginning of deformation to the fracture. The final value of D and m were found when a reasonable agreement between the experimental and numerical results was achieved.

Results and Discussion

Experimental results. The cutting and radial forces during dry and cryogenic machining are shown in Fig. 3. The application of liquid nitrogen does not have a large influence on either the cutting or radial forces. This may be due to the fact that the liquid nitrogen was sprayed to the machined surface from the clearance side of the cutting tool. It has little influence on the temperature of the primary and secondary deformation.

The influence of edge radius on radial forces for both dry and cryogenic conditions is significant. There is a 50% increase in the radial force for both cooling conditions when the edge radius was increased from 30 μm to 70 μm . The increase in cutting force is much smaller than in the radial direction. Similar trends in forces were observed by Albrecht [16]. The larger forces especially in the radial direction were attributed to the increased ploughing effect caused by larger edge radius of the cutting tool. The increased ploughing effect may be desirable for inducing grain refinement since greater severe plastic deformation is induced on the machined surface.

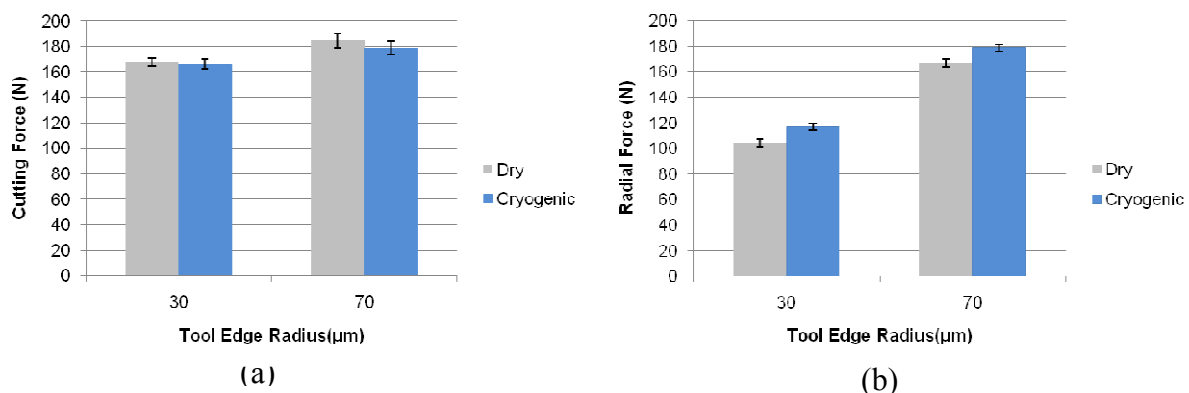


Fig. 3: Variation of measured (a) cutting and (b) radial forces with tool edge radius during dry and cryogenic machining.

The initial microstructure of the *AZ31B Mg* disc is shown in Fig. 4(a). There is no twinning in the bulk material since the as-received material is a fully annealed sheet. However, twinning is visible near the surface of the disc, which is due to the sample preparation in the machine shop where a turning operation was used as the final step in making the disc.

Significant changes on microstructures near the machined surface were observed after the machining experiments. The grain boundaries were clearly visible under dry machining using a tool with 30 μm edge radius as shown in Fig. 4(b). However, a surface layer about 8 μm thick in which grain boundaries were no longer visible at this magnification formed after cryogenic machining with the same edge radius as shown in Fig. 4(c). Below this layer, there is large amount of deformation twinning more than 50 μm away from the top surface. This shows that although application of liquid nitrogen does not have a remarkable effect on the forces, it does influence the microstructure on the surface and in the sub-surface of *AZ31B Mg* alloy significantly.

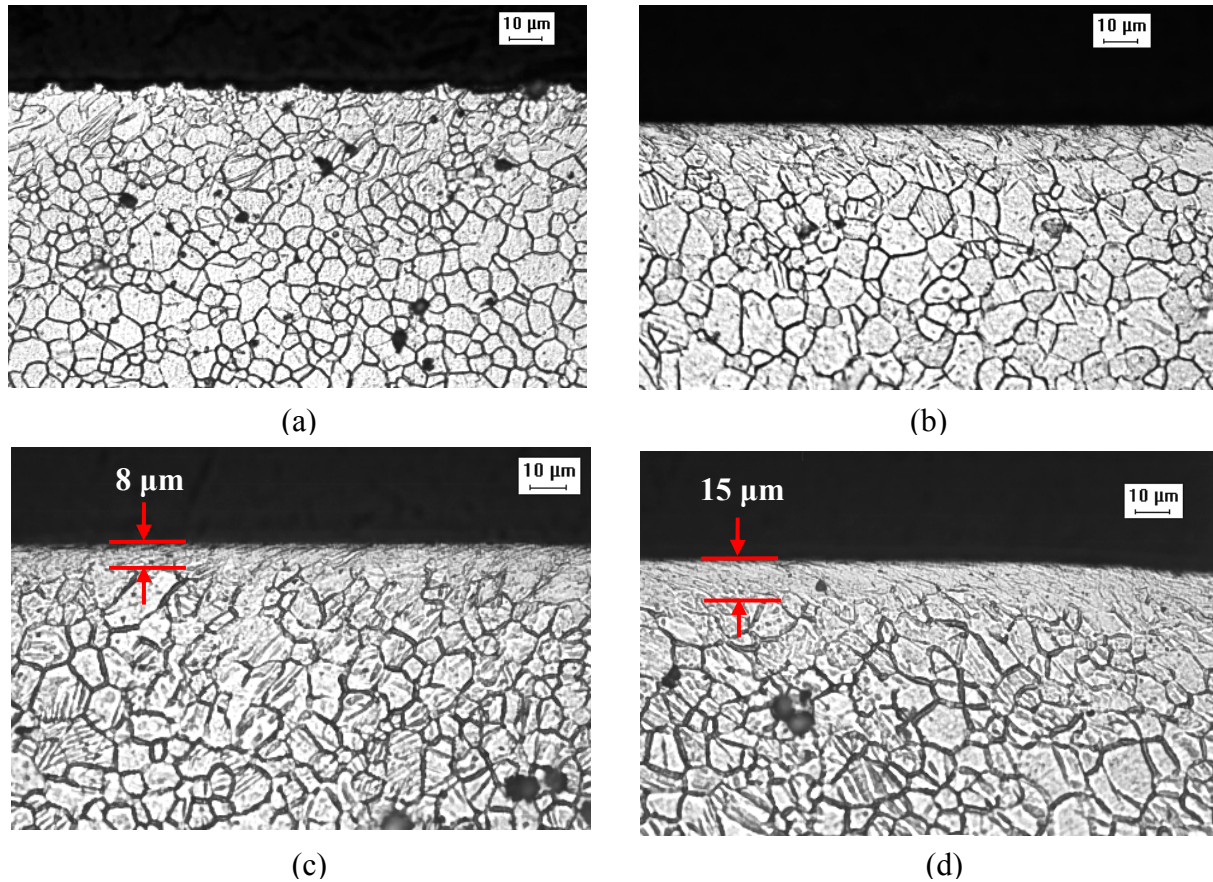


Fig. 4: Microstructure of *AZ31B* Mg discs (a) before machining and after machining: (b) dry machining, tool edge radius = 30 μm , (c) cryogenic machining, tool edge radius = 30 μm , (d) cryogenic machining, tool edge radius = 68 μm .

The thickness of the surface layer was also increased to about 15 μm when the edge radius of the tool was changed to 68 μm as shown in Fig. 4(d). Pu et al. [17] found that significant grain refinement down to about 40 nm occurred in this layer. Similar surface layers were reported after dry machining of AISI 52100 steel at low cutting speed [18] and IN 100 nickel superalloy [19].

It is noted that the grain refinement layer in the machined surface is very similar to the one at the tool-chip interface in the machined chips as shown in Fig. 5. Serrated chips were generated under both dry and cryogenic conditions. The chip morphology is very similar to the one reported by Komanduri and von Turkovich [20] in machining of titanium alloys.

The formation of adiabatic shear band is evident. The grain refinement layer which is much thicker than the one in the machined surface is formed at the chip-tool interface. The findings in this study agree with those of Calistes et al. [7] that the microstructures of the machined surface mirrored the ones in the machined chips.

The geometries of the chips under dry and cryogenic machining are compared in terms of peak, valley and pitch lengths as shown in Fig. 5(a). As shown in Fig. 6, there is little difference in the chip morphology between dry and cryogenic machining. This may be due to the fact that the liquid nitrogen was sprayed to the machined surface and has limited influence on the tool-chip interface.

Numerical simulation results. To validate the orthogonal cutting model, the predicted and experimentally measured chip morphology and forces were compared. The cutting conditions used for the validation are the same as the No.1 shown in Table 1 (dry machining, edge radius: 30 μm , cutting speed: 100 m/min, feed rate: 0.1 mm/rev).

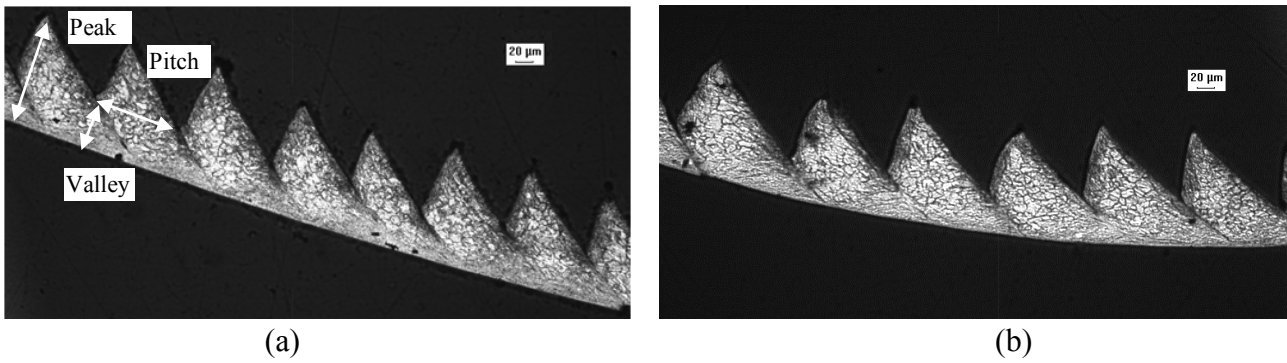


Fig. 5: Microstructures of machined chips under (a) dry and (b) cryogenic machining using cutting tools with 30 μm edge radius.

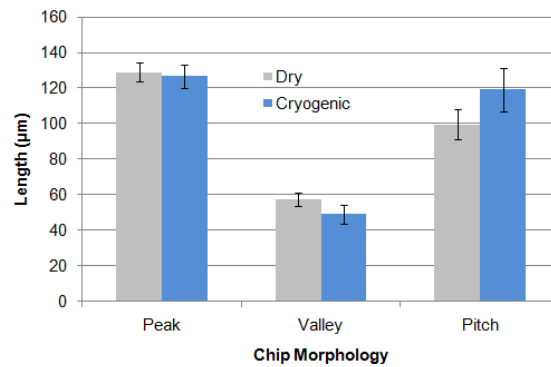


Fig. 6: Comparison of chip morphology parameters between dry and cryogenic machining using cutting tools with 30 μm edge radius.

The critical damage value (D) in Eq. 3 was reported to contribute significantly to the chip morphology and the friction coefficient (m) has significant influence on the cutting forces [14]. After the initial estimate for D was obtained, an iterative procedure was used to calibrate these two values. Typical chip morphology during the calibration phase is shown in Fig. 7. It is found that the best agreement between experimental data and simulation was achieved when D is 20 and m is 0.7. The high friction value may be due to the local adhesion between the cutting tool and the chip that occurred during dry machining of Mg alloys [21]. This conclusion is also supported by the observed material build-up on the rake side of the uncoated carbide tool used for the machining experiments.

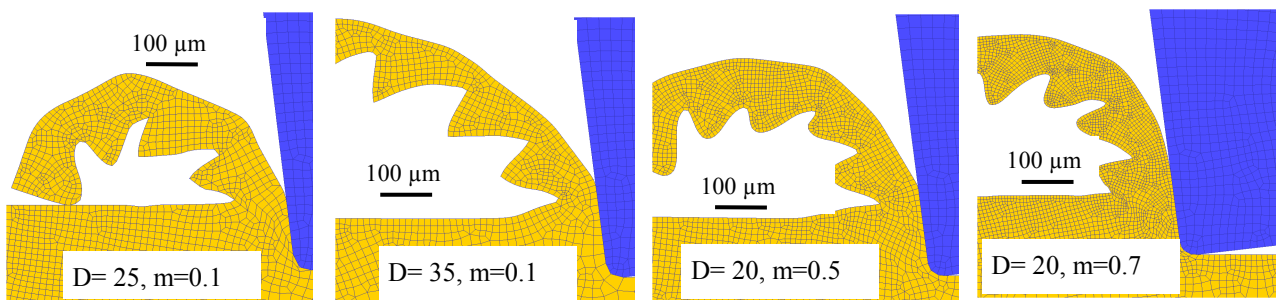


Fig. 7: Numerically obtained chip geometry at different combination of critical damage value (D) and friction coefficient (m).

Both predicted chip morphology and forces were very similar to the experimental data when $D=20$ and $m=0.7$ are used as shown in Fig. 8. Furthermore, the capability of the model to predict both cutting and radial forces for dry machining with a 67 μm edge radius tool is proved as shown in Fig. 9.

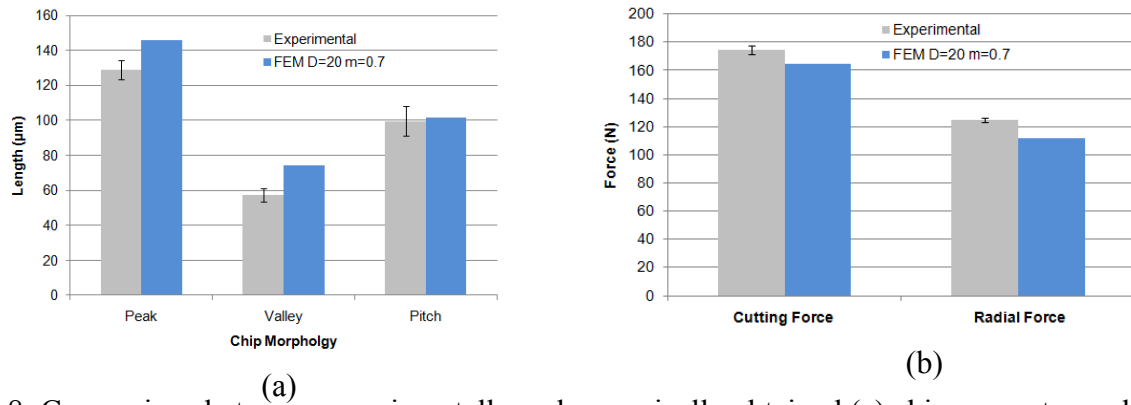


Fig. 8: Comparison between experimentally and numerically obtained (a) chip geometry and (b) forces using a tool with 30 μm edge radius under dry machining.

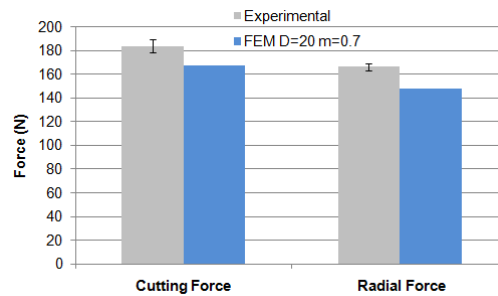


Fig. 9: Comparison between experimentally and numerically obtained forces using a tool with 67 μm edge radius under dry machining.

The onset of DRX and the grain size after DRX were reported to be a function of strain, strainrate and temperature [9] and therefore it is critical to study the distribution of these deformation parameters during machining. While these parameters, especially local values of the strain and strain-rate, are difficult to measure experimentally, the validated model developed in this study provides an alternative method to gain basic understanding of the influence of machining conditions on these deformation parameters.

The predicted distribution of effective strain under dry machining using a cutting tool with 30 μm edge radius is shown in Fig. 10. The results correlate well with the observed microstructures in the machined chip and on the machined surface as shown in Fig. 4 and Fig. 5. The formation of adiabatic shear band was evident in the FE model results.

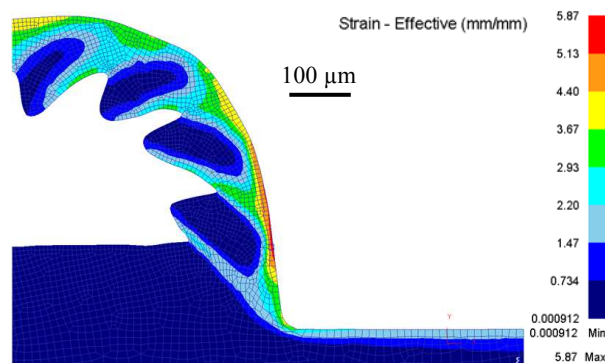


Fig. 10: Predicted distribution of effective plastic strain under dry machining (edge radius: 30 μm , cutting speed: 100m/min, feed rate: 0.1 mm/rev).

The interior of the machined chips is almost strain-free. This agrees well with the microstructures of the machined chips where the interior was almost the same as the initial material. However, very large strains were observed in the tool-chip interface and in the machined surface and sub-surface of

the workpiece. The location of the large strains agrees with the location of the grain refinement layers. The small grains observed near the surface can be explained by the DRX model proposed by Yanagimoto et al. [9] that the strain in these locations is larger than the critical strain and DRX occurs. Significant grain refinement occurs due to DRX and the grain boundaries are no longer visible under the same magnification, leading to the formation of a grain refinement layer.

A comparison of the strain distribution in the machined surface and sub-surface with different tool edge radii is shown in Fig. 11. Increased edge radius leads to larger strains which can be explained by increased ploughing effects as demonstrated by the measured forces in the previous section of this study.

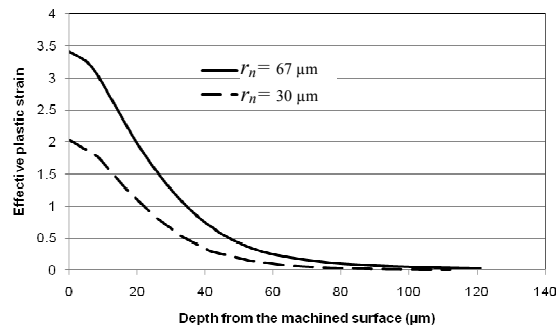


Fig. 11: Predicted distribution of effective plastic strain under dry machining with different edge radius (cutting speed: 100 m/min, feed rate: 0.1 mm/rev).

Conclusion

- Cryogenic machining leads to the formation of a grain refinement layer where nanocrystallized grain structures were observed; smaller changes occur under dry conditions.
- Larger edge radius increased the thickness of the grain refinement layer which may be due to the increased ploughing effect as evident by the larger measured forces.
- Serrated chips were formed under both dry and cryogenic machining. The formation of adiabatic shear bands was evident. Grain refinement layers similar to the ones in the workpiece were found at the tool-chip interface.
- The FE model developed can successfully predict the chip morphology and forces under dry conditions. The predicted distribution of effective strain correlates well with the observed microstructures in the machined chips and the workpiece.

In the near future, the FE model will be further developed to simulate the influence of liquid nitrogen cooling by adjusting the thermal boundary conditions based on experimentally measured temperature data during cryogenic machining. The DRX model proposed by Yanagimoto et al. [9] will also be incorporated into the FE model so that it will be capable of predicting grain size distribution on the machined surface, which will help better understanding and controlling of cryogenic machining as a novel SPD technique.

Acknowledgments

The authors would like to thank Air Products and Chemicals for providing the ICEFLY® liquid nitrogen delivery system and Kennametal for cutting tool supplies.

References

- [1] T.S. Wang, J.K. Yu, and B.F. Dong: Surf. Coat. Tech Vol. 200 (2006), p. 4777.
- [2] J.C. Villegas, L.L. Shaw, K. Dai, W. Yuan, J. Tian, P.K. Liaw, D.L. Klarstrom: Phil. Mag. Lett. Vol. 85 (2005), p. 427.
- [3] F. Witte, N. Hort, C. Vogt, S. Cohen, K.U. Kainer, R. Willumeit, F. Feyerabend: Curr. Opin. Solid St. M. Vol. 12 (2008), p. 63.
- [4] M. Alvarez-Lopez, María Dolores Pereda, J.A. del Valle, M. Fernandez-Lorenzo, M.C. Garcia-Alonso, O.A. Ruano and M.L. Escudero: Acta Biomater. Vol.6 (2010), p. 1763.
- [5] T. Balusamy, Satendra Kumar and T.S.N. Sankara Narayanan: Corros. Sci. Vol.52 (2010), p. 3826.
- [6] S. Swaminathan, M. Ravi Shankar, S. Lee, J. Hwang, A. H. King, R. F. Kezar, B. C. Rao, T. L. Brown, S. Chandrasekar, W. D. Compton, K. P. Trumble: Mater. Sci. Eng. A Vol. 410-411 (2005), p.358.
- [7] R. Calistes, S. Swaminathan, T.G. Murthy, C. Huang, C. Saldana, M.R. Shankar and S. Chandrasekar: Scripta Mater. Vol.60 (2009), p. 17.
- [8] C.I. Chang, X.H. Du, J.C. Huang: Scripta Mater. Vol.57 (2007), p. 209.
- [9] Yanagimoto J., Karhausen K: Journal of Manufacturing Science and Engineering, Vol. 120 (1998), p. 316.
- [10] J.C. Outeiro, A.M. Dias, I.S. Jawahir: CIRP Ann.-Manuf. Techn. Vol.55 (2006), p. 111.
- [11] D. Hasenpouth, "Tensile High Strain Rate Behavior of AZ31B Magnesium Alloy Sheet", Master Thesis (2010), Mechanical Engineering, University of Waterloo.
- [12] S.G. Hibbins: Proceedings of the International Symposium on Light Metals, The Metallurgical Society of CIM (1998), p. 265.
- [13] L. Filice, F. Micari, S. Rizzuti, D. Umbrello: Int. J. Mach. Tool Manu. Vol. 47 (2007), p. 709.
- [14] D. Umbrello: J. Mater. Process Tech. Vol. 196 (2008), p. 79.
- [15] M.G. Cockroft, D.J. Latham: J. I. Met. Vol. 96 (1968), p. 33.
- [16] P. Albrecht: ASME J. Eng. Ind. Vol. 81 (1960), p.348.
- [17] Z. Pu, D.A. Puleo, O.W. Dillon, Jr., I.S. Jawahir: Proceeding of Magnesium Technology 2010 (2010), TMS Annual Meeting, Seattle, WA.
- [18] A. Ramesh, S.N. Melkote, L.F. Allard, L. Riester, T.R. Watkins: Mater. Sci. Eng. A Vol.390 (2005), p.88.
- [19] Ranganath S, Guo C, Hegde P: CIRP Ann.-Manuf. Techn. Vol.58 (2009), p.77.
- [20] H.K. Tonshoff and J. Winkler: Surf. Coat Tech. Vol. 94-5 (1997), p. 610.

Modelling of Machining Operations

doi:10.4028/www.scientific.net/AMR.223

Analysis of Surface Integrity in Dry and Cryogenic Machining of *AZ31B Mg* Alloys

doi:10.4028/www.scientific.net/AMR.223.439